# Free-Energy Simulations of the Retinal Cis → Trans Isomerization in Bacteriorhodopsin[†]

Ann Hermone and Krzysztof Kuczera*

*Departments of Chemistry and Biochemistry, University of Kansas, 2010 Malott Hall, Lawrence, Kansas 66045*

*Received July 21, 1997; Revised Manuscript Received November 10, 1997*

ABSTRACT: Free-energy profiles for ground-state cis → trans isomerization of retinal in vacuum, in solution, and in the protein bacteriorhodopsin are calculated using free-energy simulations. The free-energy barriers in the protein were 9 kcal/mol for ionized Asp85 and 14 kcal/mol for neutral Asp85, significantly lower than those found in solution (18 kcal/mol) or vacuum (19 kcal/mol). Therefore, bacteriorhodopsin can be said to act as a catalyst in the isomerization. The barrier in the protein is due mainly to stabilization of the transition state through favorable nonbonded interactions with the protein part of the system, with internal strain and interactions with solvent playing minor roles. The protonated Asp85 simulation models the behavior of the system in the N → O transition. Our calculated 14 kcal/mol barrier and 4-ms relaxation time for this process are in excellent agreement with experimentally measured values of 12 kcal/mol and 5 ms, respectively. The ionized Asp85 simulation models two hypothetical processes: the N → O transition with a proton removed from Asp85 and the initial $BR_{568}$ → L transition on the ground-state energy surface. The cis−trans isomerization barrier in this system is 9 kcal/mol, the lowest of all the studied cases. The presence of the charged carboxylate group in the ionized Asp85 system leads to strong stabilization of the transition state by interactions with the surroundings and changes the distance between Asp85 and the Schiff base proton compared to the corresponding distance in the neutral Asp85 system. This suggests that the protonation of Asp85 plays an important role in regulating access to the Schiff base proton. For both Asp85 ionization states the calculated cis−trans free-energy difference was close to 0, indicating that the protein can accommodate both retinal isomers equally well. The computed negligible difference between the N and O free-energy levels is in accord with experimental data.

Bacteriorhodopsin (BR) is a bacterial membrane protein which converts light energy into the chemical energy of a proton gradient. BR contains the chromophore retinal, which is covalently bonded to Lys216 through a Schiff base linkage. In the generally accepted picture (*1*) the BR photocycle is triggered by absorption of 568-nm light leading to isomerization from *all-trans*- to 13-*cis*-retinal, followed by relaxation of the 13-cis structure, $BR_{568}$ → J → K → L; proton transfer from Schiff base to primary acceptor Asp85, L → M; proton transfer from primary donor Asp96 to Schiff base, M → N; reprotonation of Asp96 from cell interior and 13-cis → all-trans reisomerization N → O; and finally deprotonation of Asp85 and re-establishment of Schiff base−counterion complex, O → $BR_{568}$. The net effect of the photocycle is the transport of one proton across the membrane; the created proton concentration gradient is used by the organism to generate ATP (*2*−*4*). Understanding the mechanism of the BR function has profound implications in a number of areas, including the development of energy conversion technology, understanding the process of vision, and understanding biochemical active transport systems. For this reason BR has been the subject of intense experimental and theoretical study (*5*−*8*).

The initial photoisomerization on the excited-state energy surface and the subsequent ground-state relaxation to the K state are very fast, occurring on time scales of hundreds of femtoseconds and several picoseconds, respectively. These processes have been the subject of numerous computer simulations of the Schulten group (*5*, *9*). Among their findings was the suggestion that an all-trans → 13,14-dicis isomerization might initially occur, rather than all-trans → 13-cis. The simulations indicated that the former process was faster and that a 13,14-dicis conformation, unlike a 13-cis conformation, placed the Schiff base proton facing toward Asp85, the correct orientation for proton transfer (*9*). The authors postulated that, during the primary isomerization, the retinal chromophore was guided toward a 13,14-dicis conformation by an interaction with its counterion, and it isomerized to a 13-cis conformation only after deprotonation. Schulten's more recent work has centered on simulating the dark-adaptation process of BR (*10*). Several groups have used computational methods to study different aspects of BR action. Chou et al. used simulated annealing in conjunction with energy minimization to predict that the 13-cis structure of BR should be approximately 10 kcal/mol higher in energy than the all-trans state (*11*). Recently, Scharnagl et al. used classical electrostatics calculations to predict that Glu204 is the proton release group at the extracellular surface of BR (*12*); this conclusion was later supported experimentally by Brown et al. (*8*). Nina et al. used molecular dynamics

[†] Supported by NIH Grant GM-08545.

* Author to whom correspondence should be addressed. E-mail: kuczera@tedybr.chem.ukans.edu.

S0006-2960(97)01778-9 CCC: $15.00 
Published on Web 02/12/1998

simulations and energy minimizations to study hydrogen bonding of the Schiff base to water (*13*).

Our study focuses on the ground-state cis- → trans-retinal isomerization process in BR. We start by developing a consistent set of energy parameters for retinal. Next, we use these parameters to generate free-energy profiles for the all-trans → 13-cis isomerization in vacuum, in aqueous solution, and in two states of BR: with ionized and protonated Asp85. The protonated Asp85 simulation is essentially a model for the behavior of the system during the N → O transition, the second-last stage of the photocycle. The ionized Asp85 simulation provides a model of two hypothetical processes: the N → O transition with a proton removed from Asp85 and the equilibrium version of the initial $BR_{568}$ → L transition (which is in reality initiated on the excited-state energy surface). The ground-state processes are slow, involving crossing significant activation barriers; for example, the N → O transition is the slowest part of the photocycle, taking place in several milliseconds (*9*). Because of the long time scale, the isomerization processes cannot be simulated directly; we thus employ conformational free-energy simulations in which constraints are used to force the system along the reaction path. Our primary goal is to try to explain the molecular mechanism that makes the cis → trans conformational transition possible in the crowded environment of the BR protein interior. Additionally, we obtain information on the effect of the Asp85 protonation state on the N → O reisomerization, and the ground-state potential underlying the isomerization process.

The basic simulation results are free-energy profiles for rotation around the $C_{12}-C_{13}$ bond of the retinal chromophore. To better understand the role of environment, profiles are compared for isomerization in vacuum, aqueous solution, and protein matrix. Decompositions of the total free-energy changes into contributions from the different potential energy terms and parts of the system are used to obtain insight into the nature of the transition-state stabilization. The structure of the transition state is analyzed: the chromophore conformation and interactions with protein residues and with solvent water. Time series of neighboring dihedral angles are generated to verify that the isomerization was localized to $C_{12}-C_{13}-C_{14}-C_{15}$. The change in the orientation of the polyene chain is calculated and compared to experimental results.

Our calculation results show a significant lowering of the isomerization barrier in the protein relative to solution or vacuum, analogous to the stabilization of reaction transition states by enzymes (*14*). The results indicate that an all-trans → 13-cis isomerization is feasible on thermodynamic grounds. It was found that there was a small cis−trans free-energy difference in most simulations, in accord with the experimental findings of Lanyi et al. (*7*) and as postulated by Albery and Knowles (*15*). In the ionized Asp85 system, an 18° reorientation of the polyene chain was found after isomerization, in accord with the anisotropy measurements of Song et al. (*16*). The free-energy barrier of the neutral Asp85 system was in accord with the experimental findings of Lanyi et al. (*7*) and was used to calculate a time constant in agreement with the time constant measured for the N → O transition by Rothschild et al. (*17*).

Ultimately we hope our work will contribute to an improved understanding of the energy transduction mechanism in bacteriorhodopsin. Knowledge gained from the study of BR could also be applied to other, larger active transport systems such as those in the mitochondrial membrane and to the study of proteins with similar structures and chromophores, such as the vision protein opsin and G proteins.

## METHODS

The initial part of our study involved development of parameters for retinal and the retinal−lysine linkage. This work is described in detail in the Appendix. We used the CHARMM version 22 all-atom topology and parameters (*18*). All hydrogen atoms were explicitly included. In all energy evaluations an atom-based 12.0-Å nonbonded cutoff distance was employed, with a switching function between 10.0 and 12.0 Å for van der Waals terms and a shift function at 12.0 Å for electrostatics, in order to eliminate discontinuities due to the cutoff (*18*). In molecular dynamics simulations the Verlet algorithm was used with a 2-fs time step and SHAKE (*19*) constraints applied to all bonds involving hydrogen atoms.

*System Preparation*. For vacuum simulations a lysine−retinal (Lyr) system was generated, consisting of a retinal chromophore forming a Schiff base linkage with a lysine. After acetylation of the N-terminus and amidation of the C-terminus the system contained 77 atoms altogether. This system was simulated directly, starting with the coordinates of the Lyr fragment from the PDB file (*20*).

The solution simulation involved a Lyr molecule in a sphere of 19-Å radius filled with TIP3P waters (*21*). The system contained 929 water molecules and 2864 atoms altogether. The simulations used the stochastic boundary molecular dynamics (SBMD) (*22*) method. All atoms within the reaction region, comprising a 15.0-Å sphere around the origin, underwent standard Newtonian dynamics, while non-hydrogen atoms outside this sphere underwent Langevin dynamics with the random and frictional forces corresponding to a friction coefficient of 62.0 $ps^{-1}$ (*22*). The water molecules were constrained to remain inside the 19-Å sphere by a mean-field boundary potential (*22*), while the Lyr residue was kept close to the origin by application of a harmonic constraint potential with a force constant of 1.0 kcal/(mol $Å^2$) on the $C_{12}$ atom. As in the vacuum case, the PDB coordinates of the Lyr fragment were taken as the starting point of the simulation (*20*).

The starting coordinates for the simulation of retinal reisomerization in bacteriorhodopsin were based on the electron diffraction structure of Henderson et al. (*20*). Hydrogen coordinates were constructed using the HBUILD command of CHARMM (*18*). Internal water molecules were generated by overlaying a TIP3 water sphere of 23.0-Å radius on the BR structure. Twenty water molecules were left after deletion of all water molecules overlapping with the protein and all those outside the central cavity. The 10 diphosphatidyl glycerol molecules present in the PDB file (*20*) were included in the simulation system to model the presence of the lipid bilayer. The system contained 5126 atoms altogether. In the ionized Asp85 simulation the Lyr Schiff base was protonated, as were aspartic acids 96 and 115, in accord with experimental observations for $BR_{568}$ (*23*); the remaining titratable groups had standard charges, with acidic residues

(including Asp85 and Asp212) deprotonated, and basic residues protonated. The only difference in the protonated Asp85 simulation was the change of the ionization state of Asp85.

To remove any bad contacts and prepare the protein system for molecular dynamics, the structure with hydrogen atoms, internal water molecules, and lipids was minimized by 3500 steps of the adopted basis Newton−Raphson (ABNR) (*18*) algorithm with all heavy atoms fixed followed by a further 3500 steps of ABNR with all of the Cα carbon atoms of the helices under isotropic harmonic constraints with 1 kcal/(mol Å$^2$) force constants. The rms deviation from the original structure was approximately 1.6 Å for all atoms, 1.1 for atoms of the seven helices, and 1.0 for all backbone atoms. The SMBD protocol was used, in the simulations with all atoms within a reaction region of 14.0-Å radius centered at the retinal $C_{12}$ undergoing standard Newtonian dynamics. This region contained 1911 atoms. Water oxygen atoms outside the reaction region underwent Langevin dynamics with friction coefficients of 62.0 ps$^{-1}$ and were constrained to remain within a sphere of 19-Å radius by a spherical mean-field potential (*22*). All protein heavy atoms outside the reaction region underwent Langevin dynamics with 100.0-ps$^{-1}$ friction coefficients and were under isotropic harmonic constraints with a force constant of 1.0 kcal/(mol Å$^2$) (*22*). This effectively constrained the motions of all of the loops and helix ends. The lipid molecules remained fixed throughout the simulations.

*Free-Energy Simulations.* A similar protocol was followed in generating reisomerization free-energy profiles in vacuum, in aqueous solution, and in BR. Since the experimental starting structures corresponded to the all-trans state, the conformational free-energy simulations were initiated in the all-trans → 13-cis direction.

In each case the value of the $C_{12}-C_{13}-C_{14}-C_{15}$ dihedral, further denoted by $\phi$, was initially reset to 180°. The system was next heated to 300 K by random velocity assignments over 10 ps and equilibrated for 10 ps at 300 K with $\phi$ fixed using the TSM protocol of Tobias and Brooks (*24*). The all-trans → 13-cis transition was next performed in 10 windows corresponding to $\phi$ values of 180°, 160°, ..., 20°, 0°. Each "window" consisted of 20 ps of equilibration, and 40 ps of dynamics with fixed $\phi$. In vacuum, transitions between windows were generated simply by resetting the coordinates. In the crowded solution and protein environments, the 20° change in $\phi$ was broken down into 10 stages consisting of a 2° $\phi$ shift and a brief energy minimization with $\phi$ fixed at the current transient value. To examine the transition state of the system, a $\phi = 90°$ window was added, by using the coordinates generated during the $\phi = 100°$ window and gradually rotating $\phi$ to 90°. To check the consistency of the results, the transition was simulated in the reverse 13-cis → all-trans direction in an analogous way.

In the case of the protonated Asp85 simulation, we found exceptionally large differences between the forward (1: trans → cis) and reverse (2: cis → trans) simulations. Inspection of structures indicated a transition with the orientation of the Schiff base proton changing abruptly from facing Asp85 and the extracellular environment in the 120° window to facing Asp96 and the cytoplasm in the 100° window. Since we expected that the PDB structure, corresponding to $BR_{568}$, might not be the best model for the N and O states, we performed a third and a fourth free-energy simulation on the protonated Asp85 system, bringing the system back (3: trans → cis) and reversing it again (4: cis → trans). Simulations 3 and 4 of this series had reduced hysteresis compared to 1 and 2. Also, the structural changes generated in simulation 2 persisted in 3 and 4. We thus decided to report the results of simulations 3 and 4 as the forward and reverse simulations for protonated Asp 85, respectively. In these simulations the Schiff base proton was oriented toward Asp96 on the cytoplasmic side. Since the protonated Asp85 might behave similarly to Asn, such an orientation is in agreement with the results of Kataoka et al. (*25*), who found that in D85N/D96N BR mutants the Schiff base proton had access to the cytoplasm.

The symbol $\Delta G$ is used for the calculated free-energy differences. The SBMD method is expected to give free energies intermediate between Gibbs and Helmholtz values; the differences between $\Delta A$ and $\Delta G$ for the processes considered are expected to be small. The average temperatures of the simulations were 300 ± 20 K in vacuum, 290 ± 5 K in solution, and 280 ± 4 K in the protein environment.

The free-energy simulations used the conformational free energy from thermodynamic integration (CFTI) (*26*) method in which the derivative of the free energy $G$ with respect to a conformational coordinate $\phi$ is evaluated as the average of the corresponding derivative of the potential energy $U$ over conformations with fixed $\phi$ (*27*, *28*):

$$\frac{\partial G(\phi)}{\partial \phi} = \left\langle \frac{\partial U(\phi)}{\partial \phi} \right\rangle_{\phi} \qquad (1)$$

We evaluated averages $\partial U(\phi)/\partial\phi$ directly within each simulation window. The free-energy profiles $G(\phi)$ were calculated by numerical integration with linear interpolation of the derivatives, taking the $\phi = 180°$ state as the reference. Taking advantage of the linear relationship between the free energy $G$ and the potential energy $U$ in eq 1, the free-energy profiles were decomposed into contributions from internal strain (due to bond, angle, Urey−Bradley, dihedral, and improper dihedral deformations) and nonbonded interactions (van der Waals and electrostatic terms). The nonbonded component was further split into interactions of retinal with the protein and solvent parts of the system.

The values of $\partial U/\partial\phi$ were calculated every 0.02 ps. Cartesian coordinates of the system were saved for analysis and decompositions every 0.04 ps. Statistical errors of the averages were calculated as standard deviations of the mean of block averages, with the data divided into 20 blocks of equal size. Statistical errors of the free-energy profiles were determined by error propagation (*29*); errors of free-energy barriers and cis−trans free-energy differences varied from ca. 0.1 kcal/mol in vacuum to ca. 1 kcal/mol in the protein. Another measure of the error is provided by the hysteresis, given as half the difference between forward and reverse simulation results. Typical hysteresis values in the protein were 1−2 kcal/mol for barriers and 1 kcal/mol for cis−trans free-energy differences.

To compare with some experimental results, the free-energy barriers $\Delta G^{\ddagger}$ were converted to approximate rate constants $k_r$ and time scales $\tau$ using the formula

$$1/\tau = k_r = \nu e^{-\Delta G^{\ddagger}/(k_B T)} \qquad (2)$$

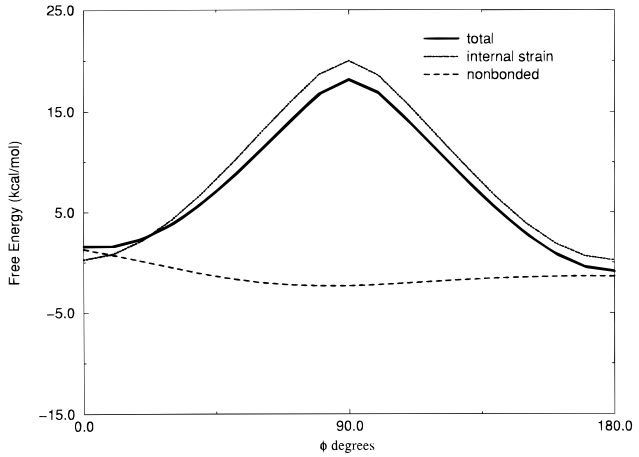


FIGURE 1: Free-energy profile for Lyr all-trans → 13-cis isomerization in vacuum. The total free-energy, as well as its internal strain and nonbonded components, is shown.

where $\upsilon$ is the average crossing frequency, $k_B$ is the Boltzmann constant, and $T$ is the absolute temperature. Transition-state theory, corresponding to the gas phase or condensed phase in the low-viscosity limit, gives $\upsilon = k_BT/h \approx 6$ ps$^{-1}$ at 300 K, with $h$ = the Planck constant (*30*). Detailed microscopic simulations predict $\upsilon \approx 2$ ps$^{-1}$ for processes in the protein interior (*31*). We have used the transition-state theory value to estimate time scales of processes from barriers; this value is also used in estimating barriers from experimental relaxation times (*2*). The detailed choice of the prefactor is not crucial due to the approximate nature of our numerical results. Statistical errors in the calculated barrier heights of 1 kcal/mol lead to variation in the exponential $e^{-\Delta G^{\ddagger}/(k_BT)}$ by a factor of 5 at 300 K.

*Programs and Computers*. All simulations were performed using CHARMM version 22 (*18*) modified to include thermodynamic integration conformational free-energy calculations and energy minimization with holonomic constraints, as described by Kuczera (*26*). Calculations were carried out on IBM RS/6000-550 and -375 workstations at the Departments of Chemistry and Biochemistry of the University of Kansas and on the Origin2000 computer at the Kansas Center for Advanced Scientific Computing.

## RESULTS AND DISCUSSION

### *Vacuum Simulation*

The free-energy profile for the simulation of Lyr in vacuum is described in Figure 1 and summarized in Table 1. The average overall barrier height was 19.0 kcal/mol above the all-trans state. The internal strain was the dominant component, contributing 19.8 kcal/mol to the total barrier; contributions from nonbonded interactions were −0.8 kcal/mol, slightly lowering the barrier. The all-trans state was 2.6 kcal/mol more stable than the 13-cis, primarily due to more favorable intramolecular nonbonded interactions. The profiles of the forward and reverse rotations (13-cis → all-trans) had similar shapes, although some hysteresis may be seen in the cis−trans free-energy difference. Examination of time series of the polyene dihedrals showed that the isomerization occurred without a transition among the other dihedrals excluding the transition forced in $C_{12}-C_{13}-C_{14}-C_{15}$.

The structures produced during the vacuum simulations are shown in Figure 2. In the all-trans state, the polyene chain stayed essentially planar with the amide and acetate blocking groups of the lysine residue oriented toward the $C_9$ and $C_{13}$ methyl groups. In the transition-state ($\phi = 90°$) structure, the polyene chain remained planar from the $\beta$-ionone ring to $C_{12}$, while the lysine side chain twisted, becoming perpendicular to the rest of the polyene chain. In the 13-cis structure the polyene chain was again planar, with the acetate and amide blocking groups oriented toward the $C_9$ and $C_{13}$ methyls.

### *Solution Simulation*

The free-energy profile for the solution simulation is described in Figure 3 and Table 1. The overall barrier height was 17.7 kcal/mol over the all-trans state, with a cis−trans difference of 0.2 kcal/mol. The internal strain component dominated the barrier and was similar to the vacuum value. The total barrier in solution was slightly lower relative to vacuum due to preferential solvation of the transition state. Overall, the nonbonded component of the free-energy accounted for a stabilization of approximately 1.8 kcal/mol. There were about 5 water molecules within 3.5 Å of the Schiff base in the all-trans, 13-cis, and transition-state ($\phi = 90°$) structures. These small differences in solvation led to essentially no contributions from solute−solvent interactions to the barrier and cis−trans free-energy difference. The solution profile exhibited quite low hysteresis, with very similar results in the forward and reverse directions.

In the solution structures of Lyr shown in Figure 4 the acetate and amide blocking groups are folded on one side of the Schiff base, with the $C_{13}$ methyl group pointing in the opposite direction. In the all-trans structure, the blocking groups are oriented away from the $C_9$ and $C_{13}$ methyls, with the $C_{13}$ methyl leaning slightly in the opposite direction. In the 13-cis structure the $C_9$ and $C_{13}$ methyl groups remain planar.

### *Simulations in the Protein Environment*

The free-energy profiles for the protein simulations are described in Figures 5 and 7 and Table 1.

*Ionized Asp85*. The ionized Asp85 simulation provides a model of two hypothetical processes: the N → O transition with a proton removed from Asp85 and the "equilibrium version" of the initial $BR_{568}$ → L transition, which in reality is initiated on the excited-state energy surface. In the ionized Asp85 system, the isomerization barrier height was ca. 9 kcal/mol over the all-trans state, with a cis−trans difference close to 0. The internal strain component of the free-energy was slightly higher than found in the vacuum and solution simulations. However, the total free-energy barrier for reisomerization within the protein was lowered approximately by 10 kcal/mol relative to vacuum and 9 kcal/mol relative to solution. Since the actual all-trans → 13-cis isomerization involves the electronically excited state, there is no valid experimental measurement for comparison. Due to the approximate methods used in parameter development (see Appendix), the relative shifts in the isomerization barrier between protein, solution, and vacuum are more reliably determined than the absolute values themselves. However, the absolute barrier heights found here appear reasonable in

Table 1: Free-Energy Barriers and Cis−Trans Free Energy Differences with Components

| | $\Delta G^{\ddagger}$ | | | | | $\Delta G_{ct}$ | | | | |
|---|---|---|---|---|---|---|---|---|---|---|
| | | | nonbonded | | | | | nonbonded | | |
| system | total | internal strain | total | solute−solute | solvent−solute | total | internal strain | total | solute−solute | solute−solvent |
| vacuum | | | | | | | | | | |
| forward | 19.0 ± 0.1 | 20.1 ± 0.1 | −1.1 ± 0.1 | | | 3.2 ± 0.1 | 0.6 ± 0.1 | 2.6 ± 0.1 | | |
| reverse | 19.0 ± 0.3 | 19.5 ± 0.1 | −0.5 ± 0.3 | | | 1.8 ± 0.2 | −0.7 ± 0.2 | 2.6 ± 0.2 | | |
| average | 19.0 | 19.8 | −0.8 | | | 2.5 | −0.1 | 2.6 | | |
| solution | | | | | | | | | | |
| forward | 17.9 ± 0.4 | 19.6 ± 0.1 | −1.7 ± 0.5 | −0.4 ± 0.1 | −1.6 ± 0.5 | 1.4 ± 0.6 | 0.2 ± 0.1 | 1.2 ± 1.1 | 3.0 ± 0.1 | −1.7 ± 0.6 |
| reverse | 17.4 ± 0.6 | 19.3 ± 0.6 | −1.8 ± 0.5 | − 0.5 ± 0.1 | −1.0 ± 0.5 | −1.1 ± 0.5 | 0.0 ± 0.2 | −1.1 ± 0.5 | 2.0 ± 0.2 | −3.1 ± 0.2 |
| average | 17.7 | 19.5 | −1.8 | −0.5 | −1.3 | 0.2 | 0.1 | 0.1 | 2.5 | −2.4 |
| protein | | | | | | | | | | |
| Asp85−[a] | | | | | | | | | | |
| forward | 11.0 ± 0.5 | 20.7 ± 0.2 | −9.7 ± 1.0 | −7.6 ± 1.0 | −2.1 ± 0.4 | 1.5 ± 0.6 | −0.4 ± 0.3 | 1.9 ± 1.2 | 5.0 ± 1.2 | −3.1 ± 0.5 |
| reverse | 7.0 ± 1.4 | 21.6 ± 0.2 | −14.6 ± 1.4 | −12.5 ± 1.4 | −2.1 ± 0.6 | −2.5 ± 1.2 | −1.1 ± 0.2 | −1.4 ± 1.2 | 3.1 ± 1.2 | −4.5 ± 0.5 |
| average | 9.0 | 21.2 | −12.2 | −10.1 | −2.1 | −0.5 | −0.8 | 0.3 | 4.1 | −3.8 |
| Asp85H[b] | | | | | | | | | | |
| forward | 16.4 ± 0.4 | 17.3 ± 0.1 | −0.8 ± 0.9 | 8.9 ± 1.0 | 8.0 ± 0.9 | −2.5 ± 0.6 | −4.4 ± 0.1 | 6.9 ± 1.0 | 3.0 ± 1.3 | 3.9 ± 1.1 |
| reverse | 12.3 ± 0.7 | 17.5 ± 0.1 | −5.2 ± 1.4 | −3.7 ± 1.0 | −1.5 ± 1.4 | −1.8 ± 0.6 | −4.8 ± 0.1 | 3.0 ± 1.2 | 6.9 ± 1.2 | −3.9 ± 1.2 |
| average | 14.3 | 17.4 | −3.0 | −6.3 | 3.3 | 0.4 | −4.6 | 5.0 | 5.0 | 0.0 |

[a] Ionized Asp85. [b] Neutral Asp85.

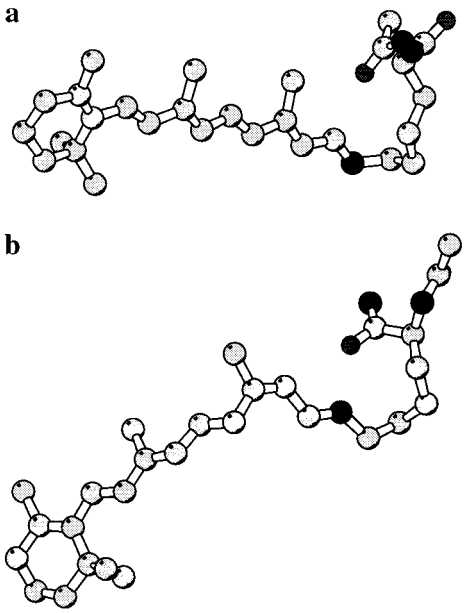


FIGURE 2: Structure of Lyr in vacuum free-energy simulation: (a) all-trans, $\phi = 180°$; (b) 13-cis, $\phi = 0°$.

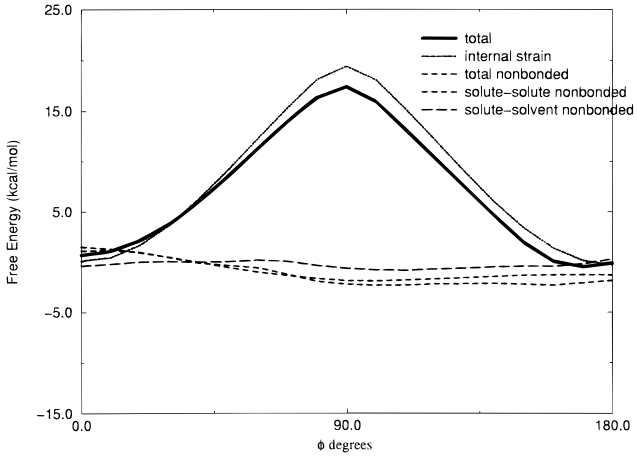


FIGURE 3: Free-energy profile for Lyr all-trans → 13-cis isomerization in aqueous solution. The total free-energy, as well as its internal strain and nonbonded components, is shown. The nonbonded component is further decomposed into contributions from interactions of Lyr with the rest of the protein and with the solvent water.

view of the good agreement with experimental data found in the neutral Asp85 simulations described in the following section. The isomerization barrier is dominated by an internal strain contribution of 21 kcal/mol; this is 1−2 kcal/mol higher than found in solution and vacuum. Ninety-nine percent of the internal strain was due to dihedral deformation. Favorable nonbonded interactions with the protein of −10 kcal/mol are the main effect responsible for the low isomerization barrier; a smaller favorable contribution of −2 kcal/mol is due to interactions with the solvent.

The cis−trans free-energy difference was close to 0, suggesting that the protein can equally well accommodate both retinal conformers without the large-scale structural change. The overall cis−trans free-energy difference consisted of two opposing effects: ca. -4 kcal/mol from interactions with solvent water and ca. 4 kcal/mol from interactions with the protein. The fact that the cis state has more favorable interactions with water than the trans state seems reasonable in view of the fact that the different proton-transfer steps of the photocycle which involve the water take place with retinal in the the cis conformation (*32*). In the actual photoinduced nonequilibrium $BR_{568} \rightarrow L$ process, experimental evidence suggests that the L intermediate lies 5−6 kcal/mol above the $BR_{568}$ state (based on Figure 7 of Váro and Lanyi (*7*)). Our simulations suggest that this effect is due to the nonequilibrium nature of the $BR_{568} \rightarrow L$ transition in the photocycle.

Asp85 is believed to be deprotonated at the start of the photocycle, and to serve as part of a "complex counterion" for the retinal Schiff base (*33*). With a distance of 1.7 Å between the Schiff base proton and the Asp85 carboxylic oxygen, Asp85 did seem to serve as a counterion in our system at $\phi = 180°$. During the isomerization, the Schiff base proton moved away from Asp85, reaching a distance of 3.5 Å for $\phi = 0°$, approaching closer to Asp96, which lies to the cytoplasmic side of Lyr.

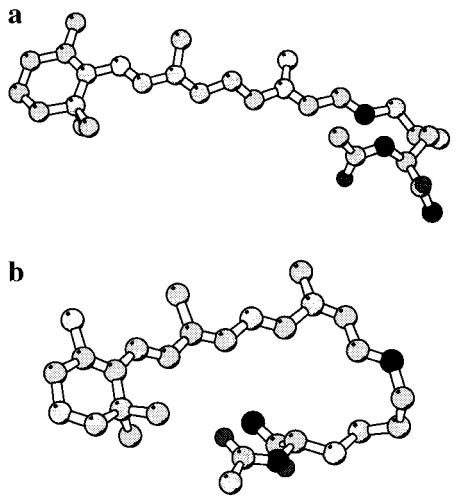


FIGURE 4: Structure of Lyr in aqueous solution free-energy simulation: (a) all-trans, $\phi = 180°$; (b) 13-cis, $\phi = 0°$.

Since in the simulations the dihedral angle was rotated gradually, the resulting 13-cis structure would correspond to an L (or M) photocycle intermediate. The polyene chain of retinal was found to have reoriented by 18° in the all-trans → 13-cis isomerization. This result is in excellent agreement with the 17° reorientation of the chromophore transition dipole in the $BR_{568}$ → L transition found in fluorescence anisotropy measurements by Song et al. (*16*).

The value of the $C_{13}-C_{14}-C_{15}-N$ dihedral angle changed gradually from 165° at $\phi = 180°$ to −127° at $\phi = 0°$ in the simulation. Our results indicate that on structural and thermodynamic grounds an all-trans → 13-cis transition is a feasible initial stage of the BR photocycle, and there is no need to invoke a 13,14-dicis intermediate. Such an intermediate might still be advantageous at other stages of the photocycle, for example, in the proton-transfer processes. The remaining polyene dihedrals also show small thermal fluctuations without conformational transitions, indicating that the retinal structural changes are localized to the $C_{12}-C_{13}$ double bond, in agreement with experimental observations.

The structure from the ionized Asp85 free-energy simulation is shown in Figure 6a,b. For $\phi = 180°$ the polyene chain is slightly bent, as in solution. The lysine side chain is oriented toward the cytoplasmic side of the membrane. The Schiff base proton is approximately 1.7 Å from atom OD1 of the carboxylic acid of Asp85. Lyr is surrounded on three sides by residues Thr89, Thr90, Thr142, and Tyr185. Thr89 is closest to the Schiff base proton, at about 4.7 Å away. Thr89 was found in previous simulations to stabilize the retinal reisomerization by hydrogen bonding to the Schiff base proton (*9*). However, in our simulations the hydroxyl group of Thr89 is only 0.6 Å closer to the Schiff base proton in the $\phi = 90°$ window than in the $\phi = 180°$ window. Several reasons may be responsible for this discrepancy. First, the Thr89 interaction could be a property of the fast nonequilibrium isomerization, as simulated by Schulten *et al.*, rather than of the slow equilibrium transition described by our simulations. Second, we use a starting structure of BR that is considerably refined compared to that employed by Zhou et al. (*9*). The changes include different positions of Asp115, Met118, and helix D; the loop regions were also determined experimentally, rather than by modeling. Finally, the different behavior of Thr89 could be due to some of the differences in the molecular models used.

*Neutral Asp85*. The free-energy profile for the neutral Asp85 isomerization is shown in Figure 7 and summarized in Table 1. As discussed previously, this simulation is designed to model the N → O transition of the BR photocycle.

In the neutral Asp85 system, the free-energy barrier for cis−trans isomerization was 14 kcal/mol over the all-trans state and the cis−trans free-energy difference was close to 0. These results are in good agreement with the experimental data of Lanyi et al., who found an N → O barrier of about 12 kcal/mol, with the N and O free-energy levels lying close

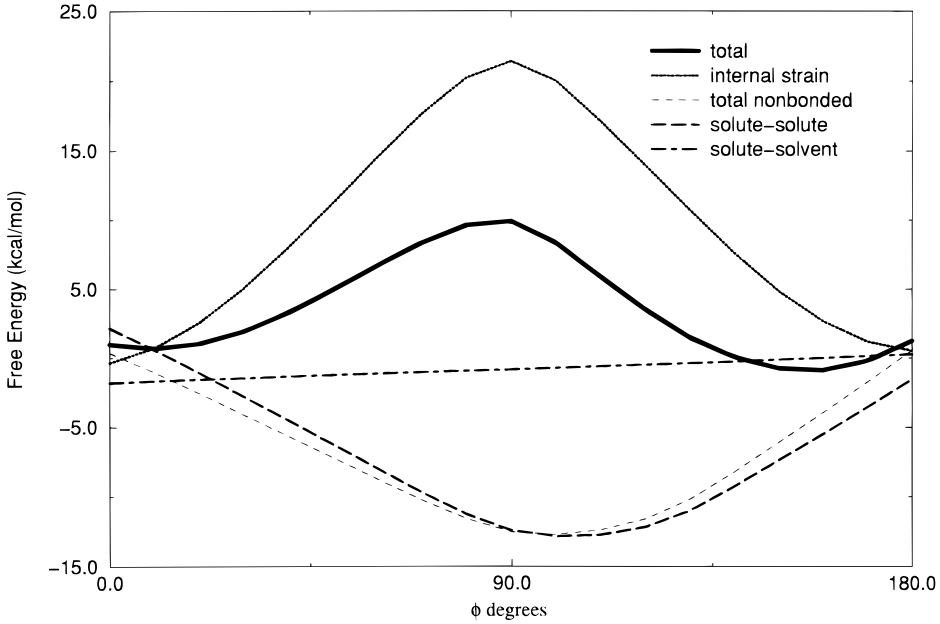


FIGURE 5: Free-energy profile for Lyr all-trans → 13-cis isomerization in bacteriorhodopsin, ionized Asp85. The total free-energy, as well as its internal strain and nonbonded components, is shown. The nonbonded component is further decomposed into contributions from interactions of Lyr with the rest of the protein and with the solvent water.

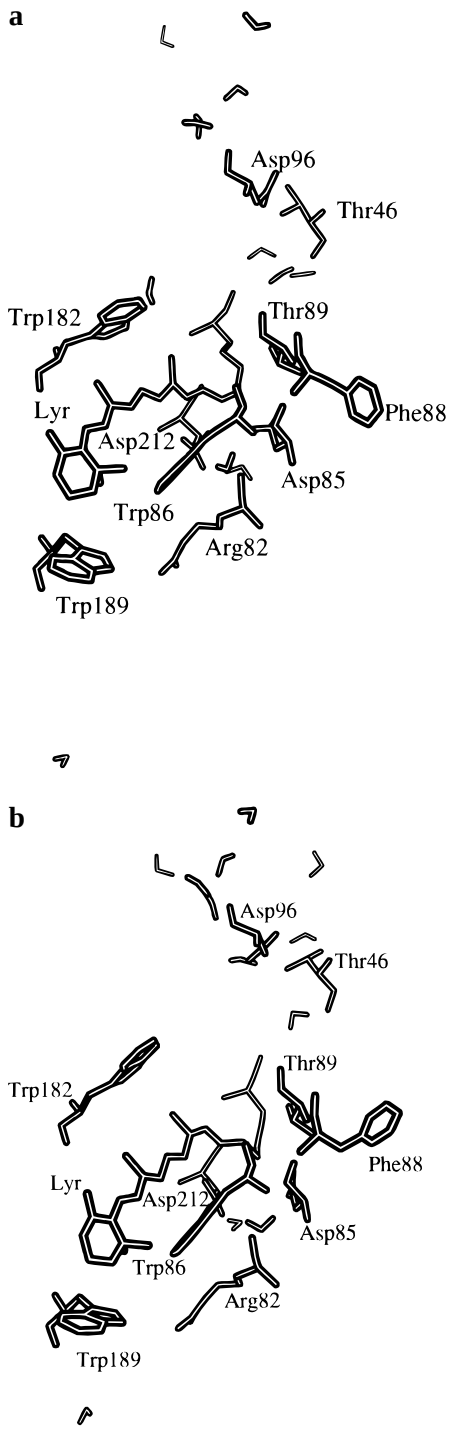


FIGURE 6: Structure of Lyr and important BR residues in ionized Asp85 free-energy simulation: (a) all-trans, $\phi = 180°$; (b) 13-cis, $\phi = 0°$.

to each other (*7*). Also, the transition-state theory relaxation time $\tau$ corresponding to a barrier of 14 kcal/mol at 300 K is 4 ms, comparable to the 5 ms measured experimentally for the N → O transition (*17*). Due to the approximate way in which we have parametrized the rotation barrier and the further approximations involved in converting barriers to time scales, this excellent agreement between simulation and experimental results is partly fortuitous. However, it is clear that our model correctly describes the overall energetics and time scale of the reisomerization. As in the ionized Asp85 simulation, we find a lowering of the isomerization barrier in the protein compared to solution or vacuum.

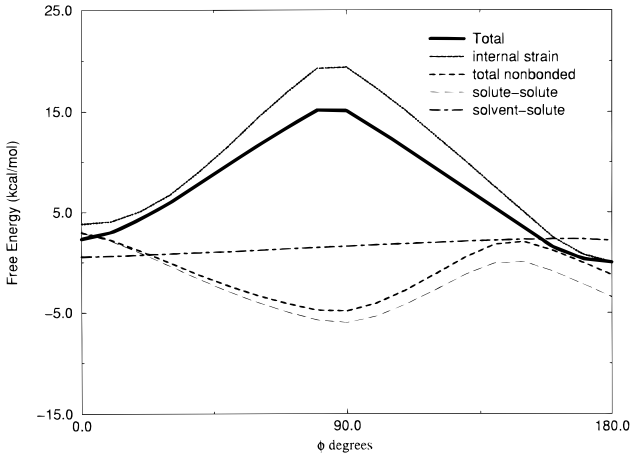


FIGURE 7: Free-energy profile for Lyr all-trans → 13-cis isomerization in bacteriorhodopsin, neutral Asp85. The total free-energy, as well as its internal strain and nonbonded components, is shown. The nonbonded component is further decomposed into contributions from interactions of Lyr with the rest of the protein and with the solvent water.

In the neutral Asp 85 system the internal strain component of the barrier was 17 kcal/mol, somewhat lower than in vacuum, solution, or ionized Asp85 cases. Again, the dihedral deformation energy dominated the internal strain, accounting for 100% of this component. The transition state is stabilized by ca. −3 kcal/mol through nonbonded interactions with the surroundings. The transition-state stabilization is due to strong favorable interactions with the protein (−6 kcal/mol), while interactions with the solvent water are unfavorable (3 kcal/mol). Interestingly, the internal strain component of the free-energy stabilizes the 13-cis state about 5 kcal/mol relative to the all-trans state, suggesting that the protein has found a more stable conformation in the 13-cis state.

As seen from comparing Figures 6 and 8, when Asp85 is ionized, the flexible lysine side chain extends toward Asp85, while in the neutral Asp85 system the distance between the deprotonated carboxylate oxygen (Asp85 OD1) and the Schiff base proton is approximately 5.5 Å in the all-trans state, about 4.0 Å further away than the ionized Asp85 all-trans window. This shift is in agreement with the expected weaker electrostatic interactions between the Schiff base and Asp85 in the neutral system. This effect can be seen in both the cis and trans states of the molecule. The position of the $\beta$-ionone ring is also shifted away from Asp85, in relation to the Asp85 system.

The reorientation of the polyene chain found in the isomerization simulation with neutral Asp85 was 12°. This is in qualitative agreement with the results of Song et al., who found that retinal essentially returns to its initial orientation in the O state (*16*). Detailed comparisons with experiment are difficult, since the orientation in the N state is unknown.

As mentioned earlier, after reisomerization from 0° to 180°, the Schiff base proton of the neutral Asp85 system faces the cytoplasmic domain, in contrast to the ionized Asp85 system. This is in agreement with the results of Kataoka et al. (*25*), who found that in D85N/D96N BR mutants the acceleration of azide on proton transport suggested that in both unphotolyzed and photoexcited systems the Schiff base proton had access to the cytoplasm. The photoelectric signal of D85N mutants (*34*) and the fact that

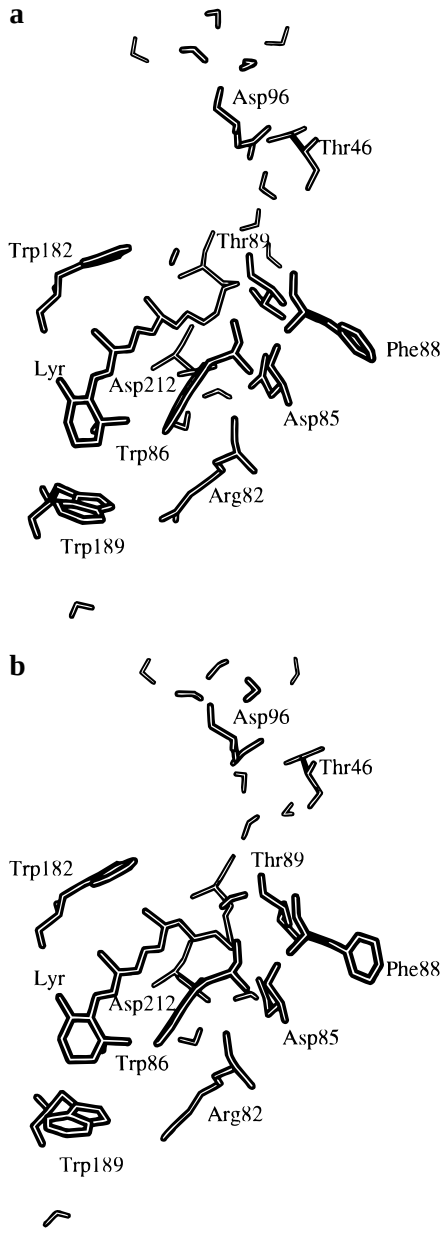


FIGURE 8: Structure of Lyr and important BR residues in neutral Asp85 free-energy simulation: (a) all-trans, $\phi = 180°$; (b) 13-cis, $\phi = 0°$.

D85N mutants pump no protons (*35*) also suggest that the release of protons is to the cytoplasm. These results suggest that the access of the Schiff base proton to the cytoplasmic and extracellular domains is regulated by the protonation state of Asp85 as suggested by Kataoka et al. (*25*). Thr89 is thought to be important in stabilizing the retinal reisomerization (*9*) by hydrogen bonding to the Schiff base proton. In the neutral Asp85 simulation the distance between the important Thr89 hydroxyl group and the Schiff base proton is about 3.7 Å in the $\phi = 180°$ window, and it increases to about 5 Å in the $\phi = 90°$ window.

## CONCLUSIONS

We have calculated the free-energy profiles for the all-trans → 13-cis isomerization of retinal in vacuum, in aqueous solution, and in the protein bacteriorhodopsin using a new consistent parameter set. The free-energy barriers in the protein were 9 kcal/mol for ionized Asp85 and 14 kcal/mol for neutral Asp85, significantly lower than those found in solution (18 kcal/mol) or vacuum (19 kcal/mol). Therefore, bacteriorhodopsin can be said to act as a catalyst in the isomerization (*14*). For both Asp85 ionization states the calculated cis−trans free-energy difference was close to 0, indicating that the protein can accommodate both retinal isomers equally well.

The protonated Asp85 simulation models the behavior of the system in the N → O transition. Our simulations agree with experimental results in a number of details. The calculated 14 kcal/mol barrier for isomerization is close to the experimental estimate of 12 kcal/mol (*7*); the corresponding calculated first-order time constant of 4 ms is comparable to the 5-ms measured value (*17*). Our calculations indicate that favorable nonbonded interactions with the protein are the main effect responsible for the lowered isomerization barrier in the protein, with nonbonded strain and interactions with solvent playing minor roles. The 12° reorientation of the polyene chain in the simulated isomerization agrees qualitatively with the findings of Song et al. that retinal returns to its initial orientation in the O state (*16*). Finally, the computed negligible difference between the N and O free-energy levels is also in accord with experimental data (*7*). As observed by Lanyi et al., these findings are in accord with Albery and Knowles (*15*), who postulated that, in enzyme catalysis in reversible systems, free-energy differences between most intermediates should be close to 0 to prevent the accumulation of intermediate species and the resulting slowing of overall reaction rates. The photocycle remains unidirectional by virtue of the irreversible $M_1$ → $M_2$ and O → BR transitions (*7*).

The ionized Asp85 simulation models two hypothetical processes: the N → O transition with a proton removed from Asp85 and the initial $BR_{568}$ → L transition on the ground-state energy surface. The cis−trans isomerization barrier in this system is the lowest of all of the studied cases. The presence of the charged carboxylate group in the ionized Asp85 system leads to strong stabilization of the transition state by interactions with the surroundings, mainly the protein part of the system. The actual N → O transition occurs with neutral Asp85, although our simulations indicate that the isomerization barrier is lower when Asp85 is ionized. This suggests that Asp85 deprotonation might be the rate-limiting process of the second half of the photocycle. The simulation yields a reorientation of the polyene chain by 18° during the retinal isomerization very close to the experimental result of 17° for $BR_{568}$ → L (*16*). Our ground-state equilibrium simulations yield a cis−trans free-energy difference close to 0 for both ionized and neutral Asp85. The suggested excess free-energy level in the L photocycle intermediate of 5−6 kcal/mol over the $BR_{568}$ ground state thus appears to be due to the nonequilibrium nature of the actual photoinduced $BR_{568}$ → L transition.

In the ionized Asp85 simulation we find a reversible shift in the distance between the Schiff base proton and the closest Asp85 carboxylate oxygen, from 1.7 Å in the all-trans state to 3.5 Å in 13-cis; the Schiff base proton also changes orientation from the extracellular (Asp85) to the cytoplasmic side (Asp96). In the neutral Asp85 simulation the distance between the Schiff base hydrogen and the carboxylic acid remains above 3.7 Å throughout. The different Schiff base to Asp85 distance in the neutral Asp85 system suggests an

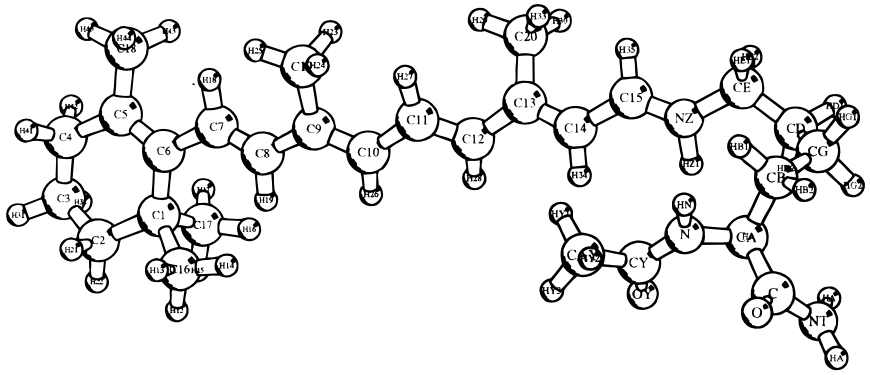


FIGURE 9: Atom-naming convention in lysine−retinal.

important role for the protonation state of Asp85 in regulating the change of access of the Schiff base proton. The orientation of the Schiff base proton in the neutral Asp85 system was found to be mainly to the cytoplasmic domain, in agreement with Kataoka et al., who found that, in a D85N mutant, proton release was always to the cytoplasm, suggesting that Schiff base orientation was always to the cytoplasm (*25*). A change of access of the Schiff base proton during the photocycle is necessary to ensure that the flow of protons remain unidirectional.

Our simulation protocol involves a number of approximations. A single BR molecule is considered, with no external water molecules and a limited number of fixed lipid molecules. The loops and helix ends are constrained, effectively eliminating the possibility of large-scale conformational change. We find that the retinal all-trans → 13-cis isomerization can take place with reasonable energetic and structural changes, with the protein remaining close to the experimental structure (1.6-Å backbone rms deviation). Our results indicate that on structural and thermodynamic grounds an all-trans → 13-cis transition is feasible in the initial stage of the BR photocycle, and there is no need to invoke a 13,-14-dicis intermediate. Such an intermediate might still be advantageous at other stages of the photocycle, for example, in the proton-transfer processes. Future plans include simulations of systems including different protonation states of crucial residues, including Asp212 and the lysine−retinal, the concerted all-trans → 13,14-dicis transition, and the dark-adaptation process in BR.

## ACKNOWLEDGMENT

The authors wish to thank Professor Martin Karplus for making available CHARMM version 22 parameters prior to publication and the Kansas Center for Advanced Scientific Computing, the Kansas Institute for Theoretical and Computational Science and Molecular Graphics and Modeling Laboratory, at the University of Kansas for use of computer resources. The authors gratefully acknowledge support from an NIH Training Grant in Chemical Biology for A.H. (GM-08545) and from the University of Kansas General Research Fund for K.K.

## APPENDIX: FORCE FIELD PARAMETRIZATION

This Appendix briefly describes our development of parameters for retinal and the retinal−lysine Schiff base linkage within the CHARMM version 22 all-atom model (*18*).

The following new atom types were introduced into CHARMM: CT0, $\beta$-ionone dimethylated $sp^3$ carbon; CEA, CEB, polyene $sp^2$ carbons; CB, $\beta$-ionone $sp^2$ carbon; CTB, $\beta$-ionone $sp^3$ carbon; NSB, Schiff base nitrogen; and HC, Schiff base proton. To provide a general method for describing polyenes, two equivalent $sp^2$ carbons were introduced, CEA and CEB; the bond alternation was then implemented by specifying that CEA−CEA and CEB−CEB bonds have double-bond character, while CEA−CEB bonds have single-bond character (see Supporting Information). Parameters were developed by separately optimizing selected properties of model compounds: ethylene, butadiene, hexatriene, 2,5-dimethylhexatriene, octatetraene, $\beta$-ionone, and (*E*)-*N*-methyl-2-ethylidenimine.

The equilibrium bond lengths and angles were adjusted to bring the CHARMM optimized geometries of the model compounds into accord with ab initio optimized geometries and crystal structures. The normal modes were calculated, using the MOLVIB section of CHARMM (*36*). The force constants for bond, angle, dihedral, and Urey−Bradley terms were adjusted to lower the root mean square (rms) deviations between the vibrational frequencies generated by CHARMM and experimental or ab initio values.

To model the internal deformations of the polyene chain, the following conjugated polyenes were used: ethylene, butadiene, hexatriene, 2,5-dimethylhexatriene, and octatetraene. The parameters for heme vinyl groups were used as a starting point. The normal modes calculated from the MOLVIB module of CHARMM were compared to experimental frequencies, in the cases of butadiene (*37*), hexatriene (*38*), and octatetraene (*39*) and to ab initio calculations in the case of dimethylhexatriene and octatetraene. All ab initio frequencies were scaled by 0.81 to correct for systematic errors (*40*). In the end we found that the CHARMM model was not capable of giving a satisfactory description of both the longer and shorter chains from the model group, and the force constants were adjusted to give an rms value of 30 $cm^{-1}$ for two of the larger molecules, hexatriene and octatetraene. No separate special parametrization for the C═C double bond torsional potential was used; the barrier parameter $V_0$ for the $0.5V_0$ $(1.0 + \cos(2\phi))$ CHARMM dihedral deformation force field was taken from fitting CHARMM to ab initio C═C torsional frequencies.

Coordinates for the carbon skeleton of the $\beta$-ionone ring were taken from Humphrey et al. (*5*) protein data bank file. The hydrogen atoms were placed using the HBUILD command of CHARMM. After geometry optimization,

frequencies were compared to scaled ab initio 6-31G* results. To model the Schiff base linkage between retinal and Lys-216, (*E*)-*N*-methyl-2-ethylidenimine was used. Both protonated and deprotonated forms were used in optimizing the geometry and force constants. Comparisons were made to the results of quantum chemical calculations for this molecule at the 6-31G* level.

The ab initio geometry optimizations and vibrational spectra calculations were performed using the GAUSSIAN92 program (*41*) at the HF/6-31G* level. These same calculations yielded Mulliken atomic charges for the model compounds. Atomic partial charges for the retinal and Schiff base atoms were determined from these Mulliken charges after scaling down by a factor of 0.8 to compensate for systematic errors of the 6-31G* basis set (*42*) and slight modifications to comply with two CHARMM version 22 model constraints: (i) to create functional groups with integer charges (..., −1, 0, +1, ...) and (ii) to assign a uniform charge of +0.09 to aliphatic hydrogens (*18*). The partial charges of the $sp^3$ carbons of the $\beta$-ionone ring were taken directly from CHARMM alkane models. The polyene partial charges were taken from the ab initio geometry optimization calculations for octatetraene. The partial charges of the protonated Schiff base linkage were based on scaled Mulliken charges from a 6-31G* geometry optimization of (*E*)-*N*-methyl-2-ethylidenimine.

Geometry comparisons to retinal crystal structures and *ab initio* calculations are given in Tables 1−3 in the Supporting Information. The bond, angle, and dihedral parameters and partial charges used for retinal are described in the Supporting Information. The structure of protonated lysine−retinal (Lyr) is given in Figure 9.

## SUPPORTING INFORMATION AVAILABLE

Tables of experimental and calculated bond lengths and angles for retinal and bond and angle parameters and partial charges for lysine−retinal (8 pages). Ordering information is given on any current masthead page.

## REFERENCES


1. Fodor, S., Ames, J. B., Gebhard, R., van der Berg, E. M., Stoekenius, W., Lugtenburg, J., and Mathies, R. A. (1988) Chromophore structure in bacteriorhodopin's n intermediate: Implications for the proton-pumping mechanism, *Biochemistry 27*, 7097−7101.
2. Lanyi, J. (1992) Proton transfer and energy coupling in the bacteriorhodopsin photocycle, *J. Bioenerg. Biomembr. 24*, 169−261.
3. Váro, G., and Lanyi, J. K. (1990) Protonation and deprotonation of the m, n, and o intermediates during the bacteriorhodopsin photocycle, *Biochemistry 29*, 6858−6965.
4. Mathies, R. A., Lin, S. W., Ames, J. B., and Pollard, W. T. (1991) From femtoseconds to biology: mechanism of bacteriorhodopin's light-driven proton pump, *Annu. Rev. Biophys. Biophys. Chem. 20*, 491−518.
5. Humphrey, W., Logunov, I., Schulten, K., and Sheves, M. (1994) Molecular dynamics study of bacteriorhodopsin and artificial pigments, *Biochemistry 33*, 3668−3678.
6. Mathies, R. A., Cruz, C. H. B., Pollard, W. T., and Shank, C. V. (1988) Direct observation of the femtosecond excited state cis−trans isomerization in bacteriorhodopsin, *Science 240*, 777−779.
7. Váro, G., and Lanyi, J. K. (1991) Thermodynamics and energy coupling in the bacteriorhopsin photocycle, *Biochemistry 30*, 5016−5022.
8. Brown, L. S., Sasake, J., Kandori, H., Maeda, A., Needleman, R., and Lanyi, J. (1995) Glutamic acid 204 is the terminal proton release group at the extracellular surface of bacteriorhodopsin, *J. Biol. Chem. 270*, 27122−27126.
9. Zhou, F., Windemuth, A., and Schulten, K. (1993) Molecular dynamics study of the proton pump cycle of bacteriorhodopsin, *Biochemistry 32*, 2291−2306.
10. Logunov, I., Humphrey, W., Schulten, K., Sheves, M. (1995) Molecular dynamics study of the 13-cis form ($BR_{548}$) of bacteriorhodopsin and its photocycle, *Biophys. J. 68*, 1270−1282.
11. Chou, K. C., Carlacci, L., Maggiora, G. M., Parodi, L. A., Schulz, M. W. (1992) An energy-based approach to packing the 7-helix bundle of bacteriorhodopsin, *Protein Sci. 1*, 810−827.
12. Scharnagl, C., Hettenkofer, J., and Fischer, S. F. (1995) Electrostatic and conformational effects on the proton translocation steps in bacteriorhodopsin: analysis of multiple m structures, *J. Phys. Chem. 99*, 7787−7800.
13. Nina, M., Roux, B., and Smith, J. C. (1995) Functional interactions in bacteriorhodopsin: A theoretical analysis of retinal hydrogen bonding with water, *Biophys. J. 68*, 25−39.
14. Voet, D., Voet, J. G. (1990) *Biochemistry*, John Wiley and Sons, New York.
15. Albery, W. J., and Knowles, J. R. (1976) Evolution of enzymes and development of catalytic efficiency, *Biochemistry 15*, 7181−7190.
16. Song, Q., Harms, G. S., Wan, C., and Johnson, C. K. (1994) Reorientations in the bacteriorhodopsin photocycle, *Biochemistry 33*, 14026−14033.
17. Braiman, M., Bousche, O., and Rothschild, K. (1991) Protein dynamics in the bacteriorhodopsin photocycle: Submillisecond fourier transform infrared spectra of the L, M, and N photointermediates, *Proc. Natl. Acad. Sci. U.S.A. 88*, 2388−2392.
18. Brooks, B. R., Bruccoleri, R., Olafson, B., States, D., Swaminathan, S., and Karplus, M. (1983) CHARMM: A program for macromolecular energy, minimization and dynamics calculations, *J. Comput. Chem. 4*, 187−217.
19. Ciccotti, G., Ryckaert, J. P., Berendsen, H. J. C. (1977) Numerical integration of the cartesian equations of motion with constraints: molecular dynamics of n-alkanes, *J. Comput. Phys. 23*, 327−341.
20. Grigorieff, N., Ceska, T. A., Downing, K. H., Baldwin, J. M., and Henderson, R. (1996) Electron-crystallographic refinement of the structure of bacteriorhodopsin, *J. Mol. Biol. 259*, 393−421.
21. Jorgensen, W. L., Chandrasekhar, J., Madura, J. D., Impey, R. W., and Klein, M. L. (1983) Comparison of simple potential functions for simulating liquid water, *J. Chem. Phys. 79*, 926−935.
22. Brooks, C. L., III, and Karplus, M. (1989) Solvent effects on protein motion and protein effects on solvent motion. Dynamics of the active site region of lysozyme, *J. Mol. Biol. 208*, 159−181.
23. Metz, G., Siebert, F., and Engelhard, M. (1992) High resolution solid state $^{13}C$ NMR of bacteriorhodopsin: Characterization of 4-$^{13}C$ Asp resonances, *Biochemistry 31*, 455−462.
24. Tobias, D. J., and Brooks, C., III. (1990) Thermodynamics of solvophobic effects: A molecular-dynamics study of n-butane in carbon tetrachloride and water, *J. Chem. Phys. 92*, 2582−2592.
25. Kataoka, M., Kamikubo, H., Tokunaga, F., Brown, L. S., Yamazaki, Y., Maeda, A., Sheves, M., Needleman, R., and Lanyi, J. K. (1994) Energy coupling in an ion pump the reprotonation switch of bacteriorhodopsin. *J. Mol. Biol. 243*, 621−638.
26. Kuczera, K. One and multidimensional conformational free-energy simulations, *J. Comput. Chem. 17*, 1726−1749.
27. Mezei, M., and Beveridge, D. L. (1986) Free energy simulations, *Ann. N.Y. Acad. Sci. 482*, 1−23.
28. Smith, D. E., and Haymet, A. D. J. (1993) Free energy, entropy and internal energy of hydrophobic interactions: computer simulations, *J. Chem. Phys. 98*, 6445−6454.
29. Bevington, P. R. (1992) *Data Reduction and Error Analysis for the Physical Sciences*, 2nd ed., McGraw-Hill, New York.

30. Kramers, H. A. (1940) Brownian motion in a field of force and the diffusion model of chemical reactions, *Physica 7*, 284−304.
31. Northrup, S. H., Pear, M. R., Lee, C.-Y., McCammon, J. A., and Karplus, M. (1982) Dynamical theory of activated processes in globular proteins, *Proc. Natl. Acad. Sci. U.S.A. 79*, 4035−4039.
32. Zimanyi, L., Váro, G., Chang, M., Ni, B., Needleman, R., and Lanyi, J. Pathways of proton release in the bacteriorhodopsin photocycle, *Biochemistry 31*, 8535−8543.
33. Rothschild, K. (1992) FTIR difference spectroscopy of bacteriorhodopsin: Toward a molecular model, *J. Bioenerg. Biomembr. 24*, 147−167.
34. Otto, H., Marti, T., Holz, M., Mogi, T., Stern, L. Engel, F., Khorana, G., and Heyn, M. (1988) Substitution of amino acids Asp-85, Asp-212, and Arg-82 in bacteriorhodopsin affects the proton release phase of the pump and the pK of the schiff base, *Proc. Natl. Acad. Sci. U.S.A. 87*, 1018−1022.
35. Mogi, T., Stern, L. J., Marti, T., Chao, B. H., and Khorana, H. G. (1988) Aspartic acid substitutions affect proton translocation in bacteriorhodopsin, *Proc. Natl. Acad. Sci. U.S.A. 85*, 4148−4152.
36. Kuczera, K., and Wiorkiewicz-Kuczera, J. MOLVIB—a program for analysis of molecular vibrational spectra. Program available from authors upon request.
37. Panchenko, Y., Pulay, P., and Torok, F. J. (1976) The calculation of the vibrational frequencies of the cis and trans forms of glyoxal, acrolein, and 1,3 butadiene, *J. Mol. Struct. 34*, 283−289.
38. Traetteberg, M. (1968) The molecular structure of 1,3,5 trans-hexatriene, *Acta Chem. Scand. 22*, 628.
39. Hamilton, T. P., and Pulay, P. (1988) Ab initio force constants and the reassignment of the vibrational spectra of *all-trans*- and *all-cis*-1,3,5,7-octatetraene, *J. Phys. Chem. 93*, 2341−2347.
40. Foresman, J., and Frisch, A. (1993) *Exploring Chemistry with Electronic Structure Methods: A Guide to using Gaussian*, Gaussian, Inc., Pittsburgh, PA.
41. Frisch, C. M. J., Trucks, G. W., Head-Gordon, M., Gill, P. M. W., Wong, M. W., Foresman, J. B., Johnson, B. G., Schlegel, H. B., Robb, M. A., Replogle, E. S., Gomperts, R., Andres, J. L., Raghavachari, K., Binkley, J. S., Gonzalez, C., Martin, R. L., Fox, D. J., Defrees, D. J., Baker, J., Stewart, J. J. P., and Pople, J. A. (1992) *GAUSSIAN92, Revision C*, Gaussian, Inc., Pittsburgh, PA.
42. Cox, S. R., and Williams, D. E. (1981) *J. Comput. Chem. 2*, 204.

BI9717789